On the Characteristics of Helical 3-D X-ray Dark-field Imaging

Lina Felsner[1], Shiyang Hu[1], Veronika Ludwig[2], Gisela Anton[2],
Andreas Maier[1], Christian Riess[1]

[1]Pattern Recognition Lab, Computer Science, Univ. of Erlangen-Nürnberg
[2]Erlangen Centre for Astroparticle Physics, Univ. of Erlangen-Nürnberg
lina.felsner@fau.de

Abstract. The X-ray dark-field can be measured with a grating interferometer. For oriented structures like fibers, the signal magnitude depends on the relative orientation between fiber and gratings. This allows to analytically reconstruct the fiber orientations at a micrometer scale. However, there currently exists no implementation of a clinically feasible trajectory for recovering the full 3-D orientation of a fiber. In principle, a helical trajectory can be suitable for this task. However, as a first step towards dark-field imaging in a helix, a careful analysis of the signal formation is required. Towards this goal, we study in this paper the impact of the grating orientation. We use a recently proposed 3D-projection model and show that the projected dark-field scattering at a single volume point depends on the grating sensitivity direction and the helix geometry. More specifically, the dark-field signal on a 3-D trajectory always consists of a linear combination of a constant and an angular-dependent component.

1   Introduction

X-ray phase-contrast is an interferometric imaging technique that is compatible with clinical requirements. It can be implemented with a Talbot-Lau interferometer via a set of gratings between a medical X-ray source and detector (see Fig. 1). This interferometer creates an attenuation image, a differential phase image and a dark-field image. The dark-field image measures small-angle scattering of fibrous structures. The strength of the anisotropic dark-field signal depends on the relative orientation of a fiber to the gratings [1,2].

In recent years, several medical applications of the dark-field signal were investigated, for example for tumor detection, e.g., in the lung [3,4], or the anisotropic reconstruction of the brain fiber connectivity [5].

Several algorithms were proposed for anisotropic dark-field reconstruction in 2-D and 3-D [6,7,8,9,10,11]. 2-D methods [2,6] reconstruct the projection of the fiber-orientation in one plane. 3-D reconstructions are based on various models. One approach is to compute the 3-D tensor indirectly from two 2-D vectors [7], others are X-ray tensor tomography [8], to fit a scattering ellipsoid [9], or to
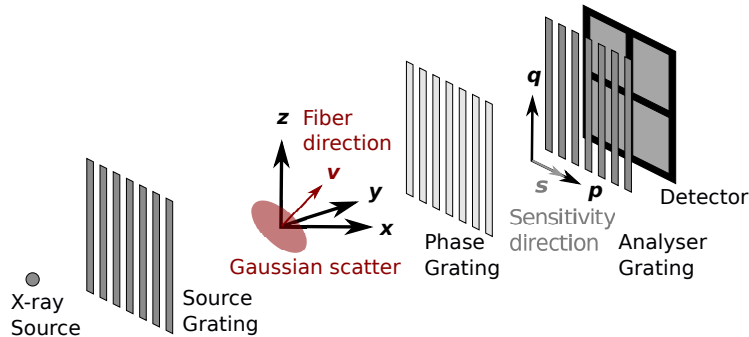
Fig. 1. Sketch of setup and coordinate systems. The global coordinate system is denoted as $\{\boldsymbol{x}, \boldsymbol{y}, \boldsymbol{z}\} \in \mathbb{R}^3$ and the detector coordinate system is given as $\{\boldsymbol{p}, \boldsymbol{q}\} \in \mathbb{R}^2$.

estimate spherical harmonics [10]. All these methods rely on iterative reconstruction. Recently, Schaff *et al.* proposed a non-iterative approach [11]. They aligned the grating bars perpendicular to the rotation axis, such that the sensitivity direction is parallel to the rotation axis. This way, the projection of the fiber onto the sensitivity direction is constant for the scan, and a standard filtered back-projection (FBP) can be used for a 2-D reconstruction. 3-D fiber orientations are then estimated by combining reconstructions from multiple trajectories. However, all these models rely on specialized, quite complex trajectories, which prohibits their use for medical applications.

In this paper, we make first steps towards a novel approach for 3-D dark-field imaging. The idea is to use a 3-D helix trajectory. While, in principle, a helix allows recovery of 3-D information, it is necessary to closely examine the associated dark-field signal model, which is subject of this work. The dark-field model and projection models in 2-D and 3-D are presented in Sec. 2. We investigate the helical trajectory in more detail. In Sec. 3, we evaluate the dark-field signal for different helical trajectories, followed by a discussion in Sec. 4.

2   Materials and Methods

The dark-field model is described below. Its characteristics in a 2-D and 3-D scanning trajectory are presented in Sec. 2.1 and Sec. 2.2, respectively.

Our examinations are based on the 3-D dark-field model proposed in [12]. However, in this work we will limit ourself to only one fiber. Moreover, we will not consider the full model, but consider only the projections of the associated Gaussian scatter function. The dark-field signal then consists of an isotropic part that is constant in all directions, and an anisotropic part that depends on the viewing and grating sensitivity direction.

The observed dark-field signal d from a single Gaussian scattering function is defined as

$$d = d_{\mathrm{iso}} + d_{\mathrm{aniso}}(\boldsymbol{s}^\top \boldsymbol{v})^2 \,, \tag{1}$$
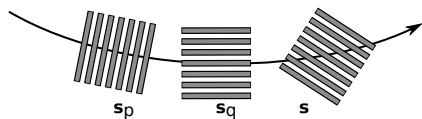
Fig. 2. Grating directions are described with respect to the trajectory.
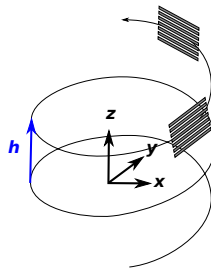
Fig. 3. Helix

where d_{aniso} describes anisotropic the scattering strength of the object, and d_{iso} the isotropic part. The anisotropic signal is modeled as the inner product of a scattering fiber vector $\boldsymbol{v}$ and sensitivity direction $\boldsymbol{s}$. In this work, we assume that $\boldsymbol{s}$ and $\boldsymbol{v}$ are normalized to 1. Both vectors are shown in Fig. 1.

2.1   Dark-field with 2-D Trajectories

Existing dark-field projections were only described for 2-D trajectories [6,11]. There, the grating alignment is either parallel to the rotation axis [6] (see Fig. 2 (left)) or perpendicular to it [11] (see Fig. 2 (middle)). For the following specific descriptions we use the coordinate system(s) defined in Fig. 1.

If the gratings are aligned parallel to the rotation axis, the sensitivity direction is parallel to the trajectory and given as $\boldsymbol{s} = (1,0)^{\top}$. The measured dark-field signal is then the projection of $\boldsymbol{v}$ in the x-y-plane. This results in a sinusoidal function that depends on the rotation angle. Since the sensitivity direction is given by the vector $\boldsymbol{p}$ (see Fig. 1) we denote this special case as $\boldsymbol{s}_p$.

If the gratings are aligned parallel to the trajectory, the sensitivity direction is parallel to the rotation axis $\boldsymbol{s} = (0,1)^{\top}$. In this case, the projection of the fiber on the z-axis is measured, which leads to a dark-field signal that is constant during tomography. This case is denoted as $\boldsymbol{s}_q$.

In principle, the gratings could also be oriented diagonally (see Fig. 2 (right)). In this case, the observed dark-field signal is a linear combination of $\boldsymbol{s}_p$ and $\boldsymbol{s}_q$. The sensitivity direction $\boldsymbol{s}$ is then given by

$$\boldsymbol{s} = A \cdot \boldsymbol{s}_p + B \cdot \boldsymbol{s}_q \ . \tag{2}$$

2.2   Dark-field with a 3-D Helical Trajectory

Unlike 2-D trajectories, the reconstruction plane of a 3-D trajectory is not necessarily perpendicular to the rotation axis. Then, the observed dark-field signal is a non-trivial linear combination of $\boldsymbol{s}_p$ and $\boldsymbol{s}_q$. We now apply this reasoning to the medically relevant special case of a helix trajectory. Here, the X-ray system is rotating around the object, with an offset along the rotation axis. The amount

of the translation along the rotation axis for one full circle (360°) is called pitch h. A schematic sketch of a helix and the corresponding pitch is shown in Fig. 3. The helix describes a continuous path, and hence for the case that the sensitivity direction is aligned with the trajectory, the sensitivity is given by

$$\boldsymbol{s} = A \cdot (1, \, 0)^\top + B \cdot (0, \, 1)^\top = (A, \, B)^\top \ . \tag{3}$$

Here, the helix-specific parameters A and B, are

$$A = -\alpha \cdot \sqrt{1 - B^2} \tag{4}$$

$$B = \beta \cdot \frac{2}{\pi} \ , \tag{5}$$

where α is the signed rotation angle between two consecutive projections and β is the signed rising angle of the helix. Thus, the behavior of the dark-field projection in a helix is defined by the sensitivity direction and the helix pitch.

3 Experiments and Results

We show the behavior of the 3-D dark-field on helix pitch and grating orientation for simulated data. The fiber in our experiments is defined by the parameters $d_{\mathrm{iso}} = 1$, $d_{\mathrm{aniso}} = 1.73 = \sqrt{3}$ and $\boldsymbol{v} = (1, 1, 1)$ and it is centered at the rotation axis. We will consider six different trajectory settings, which differ in the trajectory or the sensitivity direction. We simulate a cone-beam geometry and define the sensitivity vector $\boldsymbol{s}$ to always be perpendicular on the ray direction $\boldsymbol{r}$. This corresponds to a curved detector, which slightly simplifies the interpretation of the results. The setup geometry always has a source-isocenter distance of 600 mm and source-detector distance of 1200 mm. The 2-D circle trajectories (Fig. 4(a,b)) consist of 360° with angular increment of 1.5°. The helical trajectories (Fig. 4(c-f)) also with angular increment of 1.5°, with pitch h_1 or h_2.

Experiment 1. We investigate two cases of a circular trajectory. First, the gratings are perpendicular to the trajectory (see Fig. 4(a)), i.e., with sensitivity direction $\boldsymbol{s}_p$. Second, the gratings are parallel to the trajectory (see Fig. 4(b)), i.e., with sensitivity direction $\boldsymbol{s}_q$. The resulting dark-field signal is shown in Fig. 5 for sensitivity direction $\boldsymbol{s}_p$ in red and sensitivity direction $\boldsymbol{s}_q$ in blue. While the dark-field signal with direction $\boldsymbol{s}_p$ varies across the tomographic angles, the dark-field signal with direction $\boldsymbol{s}_q$ is constant.

Experiment 2. In this experiment, the dark-field signal for helical trajectories with different pitches are compared. We set the pitches h_1 to the detector height, $h_2 = 0.5 \cdot h_1$, and $h_3 = 2 \cdot h_1$. For gratings parallel to the trajectory, this variation of detector pitch visualized in Fig. 4(c) and Fig. 4(d). The resulting intensity variations are shown in Fig. 6 (left). Here, black, red, and blue show the intensity profiles for pitches h_1, h_2, h_3, respectively. The variations in the curves show that the amplitude, and hence the anisotropic part of the signal, increases with the pitch. However, this dependency scales not linearly. Note also that the fiber is observed over a smaller angular range with increasing pitch.
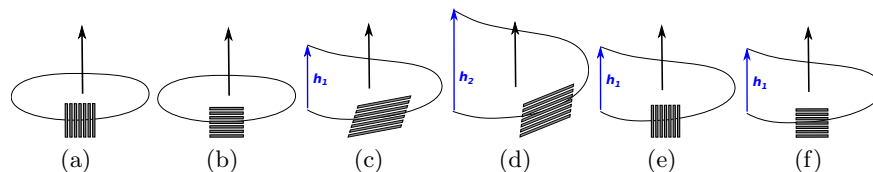
Fig. 4. Experiments. (a,b) circle trajectory (c-f) helical trajectory. For each scanning mode the grating orientation and rotation axis is shown.
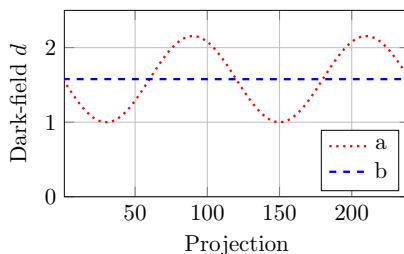
Fig. 5. Line plot of dark-field with a circular trajectory. Intensity profiles in red and blue correspond to grating orientations in Fig. 4(a) and Fig. 4(b), respectively.

Experiment 3. For pitch h_1, we evaluate the sensitivity directions shown in Fig. 4(c), 4(e) and 4(f). The resulting intensity profiles are shown in Fig. 6 (right), where the black, red, and blue curves correspond to the directions in Fig. 4(c), 4(e) and 4(f), respectively. Unlike the case of gratings parallel to the trajectory in Exp. 1, none of these grating orientations leads to a constant signal: the 3-D helix trajectory always leads to a (non-trivial) linear combination of s_p and s_q.

4   Discussion

We showed that the dark-field signal behaves differently for 2-D and 3-D trajectories. On 3-D trajectories, we necessarily observe a linear combination of the two 2-D base cases. This leads to a mixture of a constant and a varying signal component. For the particular case of a helical trajectory, we validated these findings with simulation experiments. We believe that understanding the dark-field signal in a helix opens the perspective to implement orientation-sensitive tomographic systems that are much more practical for scanning patients. As a next step the complete 3-D projection model described in [12] shall be evaluated with a helical trajectory. For future work we will investigate an algorithm that incorporates trajectory-dependent information to simultaneously reconstruct the scatter directions and isotropic signal components.

Acknowledgements.
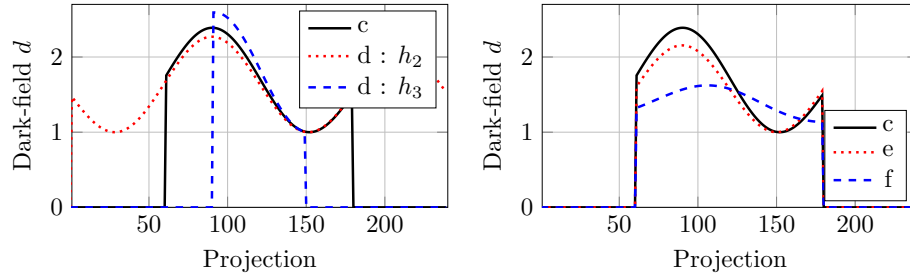
(a) Helical trajectory with different pitch. $h_2 = 0.5 \cdot h_1$ and $h_3 = 2 \cdot h_1$.

(b) Helical trajectory with different sensitivity directions.

Fig. 6. Line plot of dark-field for different helical trajectories. The corresponding grating orientations are shown in Fig. 4(c-f).

References

1. Jensen TH, Bech M, Bunk O, Donath T, David C, Feidenhans R, et al. Directional X-ray dark-field imaging. Physics in Medicine & Biology. 2010;55(12):3317.
2. Revol V, Kottler C, Kaufmann R, Neels A, Dommann A. Orientation-selective X-ray dark field imaging of ordered systems. Journal of Applied Physics. 2012;112(11):114903.
3. Scherer K, Yaroshenko A, Bölükbas DA, Gromann LB, Hellbach K, Meinel FG, et al. X-ray dark-field radiography-in-vivo diagnosis of lung cancer in mice. Scientific reports. 2017;7(1):402.
4. Hellbach K, Baehr A, Marco F, Willer K, Gromann LB, Herzen J, et al. Depiction of pneumothoraces in a large animal model using X-ray dark-field radiography. Scientific reports. 2018;8(1):2602.
5. Wieczorek M, Schaff F, Jud C, Pfeiffer D, Pfeiffer F, Lasser T. Brain connectivity exposed by anisotropic X-ray dark-field tomography. Scientific reports. 2018;8.
6. Bayer FL, Hu S, Maier A, Weber T, Anton G, Michel T, et al. Reconstruction of scalar and vectorial components in X-ray dark-field tomography. Proceedings of the National Academy of Sciences. 2014;111(35):12699–12704.
7. Hu S, Riess C, Hornegger J, Fischer P, Bayer F, Weber T, et al. 3D tensor reconstruction in X-ray dark-field tomography. In: Bildverarbeitung für die Medizin 2015. Springer; 2015. p. 492–497.
8. Malecki A, Potdevin G, Biernath T, Eggl E, Willer K, Lasser T, et al. X-ray tensor tomography. EPL (Europhysics Letters). 2014;105(3):38002.
9. Vogel J, Schaff F, Fehringer A, Jud C, Wieczorek M, Pfeiffer F, et al. Constrained X-ray tensor tomography reconstruction. Optics Express. 2015;23(12):15134–15151.
10. Wieczorek M, Schaff F, Pfeiffer F, Lasser T. Anisotropic X-ray dark-field tomography: A continuous model and its discretization. Physical review letters. 2016;117(15):158101.
11. Schaff F, Prade F, Sharma Y, Bech M, Pfeiffer F. Non-iterative directional dark-field tomography. Scientific Reports. 2017;7(1):3307.
12. Hu S, Felsner L, Maier A, Ludwig V, Anton G, Riess C. A 3-D projection model for X-ray dark-field imaging. arXiv:1811.04457; 2018.